T- and L-type calcium channels maintain calcium oscillations in the murine zona glomerulosa

Hoang An Dinh[1], Marina Volkert[1], Ali Kerim Secener[1,2,3], Ute I. Scholl[1,4] and Gabriel Stölting[1]

[1] Berlin Institute of Health at Charité – Universitätsmedizin Berlin, Center of Functional Genomics, 10115 Berlin, Germany

[2]Genomics Technology Platform, Max Delbrück Center for Molecular Medicine in the Helmholtz Association (MDC), Berlin, Germany

[3]Institute of Chemistry and Biochemistry, Department of Biology, Chemistry and Pharmacy, Freie Universität Berlin, Germany

[4]Charité – Universitätsmedizin Berlin, corporate member of Freie Universität Berlin and Humboldt-Universität zu Berlin, Department of Nephrology and Medical Intensive Care, 10117 Berlin, Germany

Abstract

The zona glomerulosa of the adrenal gland is responsible for the synthesis and release of the mineralocorticoid aldosterone. This steroid hormone regulates salt reabsorption in the kidney and blood pressure. The most important stimuli of aldosterone synthesis are the serum concentrations of angiotensin II and potassium. In response to these stimuli, voltage and intracellular calcium levels in the zona glomerulosa oscillate, providing the signal for aldosterone synthesis. It was proposed that the voltage-gated T-type calcium channel $Ca_V3.2$ is necessary for the generation of these oscillations. However, *Cacna1h* knockout mice have normal plasma aldosterone levels, suggesting additional calcium entry pathways. We used a combination of calcium imaging, patch clamp and RNA sequencing to investigate such pathways in the murine zona glomerulosa. *Cacna1h*$^{-/-}$ glomerulosa cells showed similar calcium levels as wild-type mice in response to stimulation with angiotensin II or potassium. No calcium channels or transporters were upregulated to compensate for the loss of $Ca_V3.2$. The calcium oscillations observed in the zona glomerulosa of *Cacna1h*$^{-/-}$ mice were instead dependent on L-type voltage-gated calcium

channels. Furthermore, we found these channels also in the wild-type zona glomerulosa where they can partially compensate for an acute inhibition of $Ca_V3.2$. Inhibition of both, T- and L-type calcium channels abolished the increase of intracellular calcium caused by angiotensin II. Our study demonstrates that T-type calcium channels are not required to maintain glomerulosa calcium oscillations and aldosterone production.

Introduction

The adrenal glands are a pair of endocrine organs located above the kidneys. They develop from two separate germ layers: the ectoderm forming the neuroendocrine medulla and the mesoderm that forms the steroid hormone-producing adrenal cortex. All steroid hormones are synthesized from the precursor cholesterol. The outermost zona glomerulosa (ZG) produces aldosterone, the zona fasciculata (ZF) either cortisol in humans or corticosterone in mice and the innermost zona reticularis (ZR, in humans) androgens. Aldosterone is responsible for the maintenance of blood salt levels and volume via the regulation of various ion transporters in the kidney and intestine. Aldosterone synthesis in the ZG is tightly controlled by stimuli linked to these targets, primarily the serum concentrations of potassium and angiotensin II (Ang II)[1]. Partial uncoupling of aldosterone synthesis from these stimuli results in primary aldosteronism. This condition is estimated to underly 6% of all hypertension cases in a primary care setting and is likely still vastly underdiagnosed[2].

ZG cells have a highly negative resting membrane potential that is determined by their predominant potassium conductance at rest. Binding of Ang II to its cognate receptor leads to the activation of phospholipase C and the subsequent cleavage of Phosphatidylinositol-4,5-bisphosphat (PIP_2) into inositol trisphosphate (IP_3) and diacylglycerol (DAG). This results in the depolarization of ZG cells, causing influx of calcium via voltage-gated calcium channels [3–6] and also via the release of calcium from intracellular stores elicited by IP_3[7,8]. We and others have indirectly shown that potassium only appears to modify calcium influx when the ZG is first stimulated with Ang II [9–11], likely through modifying electrical excitability.

Calcium itself is required for several key functions in ZG cells, such as the regulation of transcription factors upstream of the aldosterone synthase *Cyp11b2*[12,13] or the transport of cholesterol to the inner membrane leaflet of mitochondria for conversion into aldosterone[14]. Tight control over $[Ca^{2+}]_{int}$ is therefore key to the control of aldosterone synthesis.

Depolarizations of murine ZG cells occur in oscillations that increase upon stimulation with potassium or Ang II[15]. We and other groups have shown that also the intracellular concentration of calcium ($[Ca^{2+}]_{int}$) fluctuates with a similar pattern and frequency[5,9–11].

The original publication identifying murine ZG cells as voltage oscillators demonstrated that voltage fluctuations critically depend on the function of the T-type voltage-gated calcium channel $Ca_V3.2$ (Gene: *Cacna1h*) and specific inhibition of this channel abolished all voltage

oscillations[15]. Even before, the specific inhibition of T-type calcium channels has been proposed as a potential strategy to pharmacologically suppress aldosterone production[16]. Additionally, L-type calcium channels such as $Ca_V1.2$ and 1.3 are also known to be expressed In the adrenal gland[17–19]. These are thought to contribute to calcium influx during depolarizations[20] and gain-of-function mutations in CACNA1D (encoding $Ca_V1.3$) have been linked to primary aldosteronism[17,21].

However, despite its critical role in the electrical excitability of the ZG, $Ca_V3.2$ knock-out mice did not show altered systemic aldosterone or renin levels[11,22] nor altered responses to an infusion with Ang II[22]. The molecular mechanisms that sustain aldosterone production in $Ca_V3.2$ knock-out mice currently remain unclear. We here set out to investigate the regulation of $[Ca^{2+}]_{int}$ in the ZG of mice lacking $Ca_V3.2$ and the implications of the results on wild-type (WT) ZG function and pharmacology of the ZG.

Results

ZG cells from *Cacna1h*$^{-/-}$ mice still exhibit intracellular calcium oscillations

To study $[Ca^{2+}]_{int}$ in murine ZG cells, we stained acutely prepared slices from mouse adrenal glands with the intensiometric fluorescent calcium indicator Calbryte 520 AM (to obtain a high temporal resolution) or Fura-2 AM (to allow for absolute concentration quantification). We used WT as well as *Cacna1h*$^{-/-}$ (KO) mouse lines that we established previously[11].

When stimulated with 500 pmol/l Ang II and 4 mmol/l K^+, ZG cells in slices from WT mice responded with pronounced Ca^{2+} oscillations. As observed previously[9,11], individual transients (spikes) were homogeneous in appearance. Spikes were clustered in bursts, separated by pauses at a mostly constant baseline $[Ca^{2+}]_{int}$ (Fig. 1A). Although lacking the $Ca_V3.2$ channel, $[Ca^{2+}]_{int}$ in ZG cells from KO mice exhibited similar behavior: Homogeneous spikes, clustered into bursts (Fig. 1B).

The most prominent difference of the spiking in KO mice was the significantly increased overall number of spikes per second (activity; Fig. 1C, Supplementary Table S1). This was caused by an increased frequency of spikes within bursts (Supplementary Fig. S1A) and shorter gaps between bursts (Supplementary Fig. S1B) rather than longer bursts (Supplementary Fig. S1C).

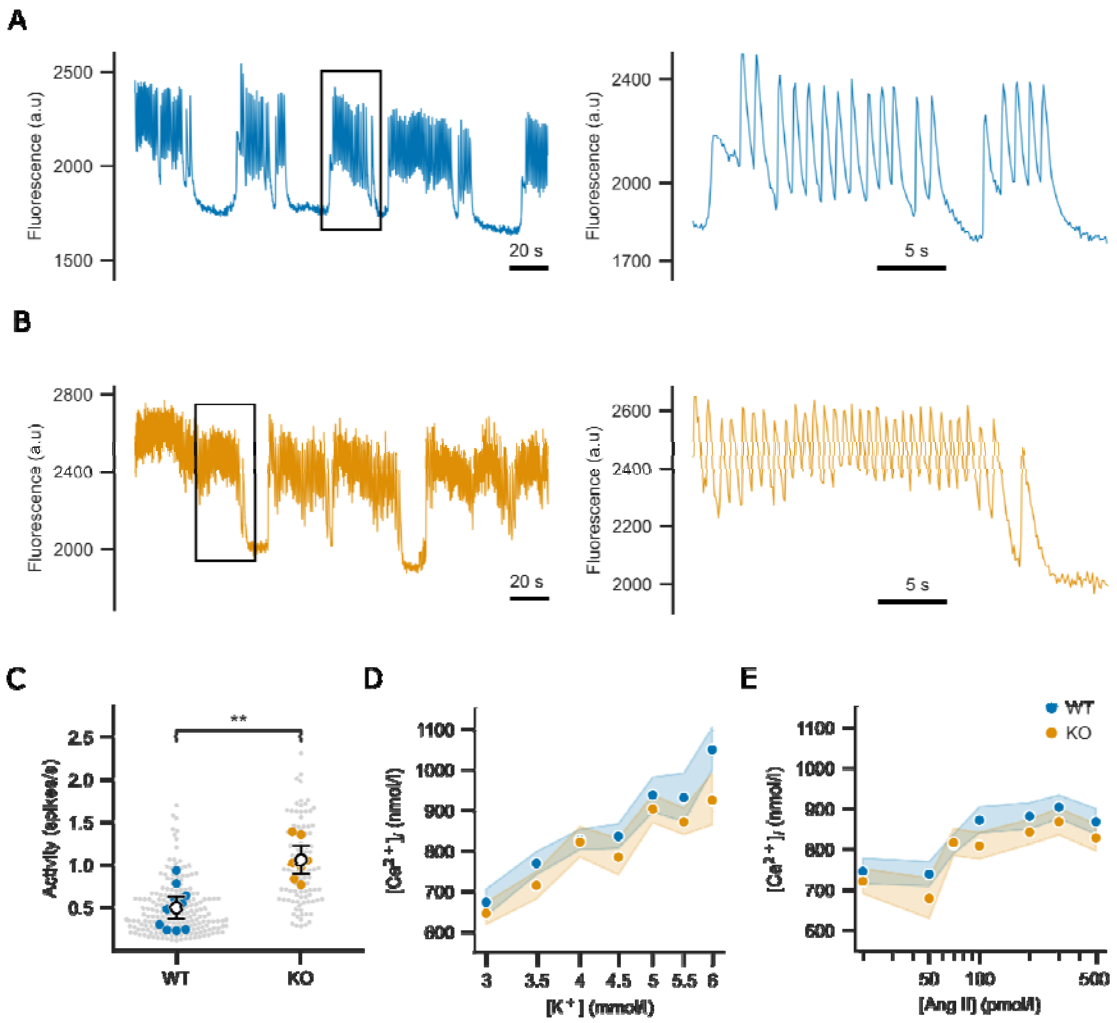

Figure 1. Calcium oscillations persist in Cacna1h$^{-/-}$ mice. (A-B) *Fluorescence signals over 3.5 min recorded from one representative ZG cell each of a WT* ***(A)*** *or KO* ***(B)*** *adrenal slice stained with Calbryte 520 AM. Cells were stimulated with 4 mmol/l K^+ and 500 pmol/l Ang II. A corresponding 30 s magnification (indicated by the black rectangle on the left) is shown on the right.* ***(C)*** *Calcium spike activity (mean number of spikes per cell and second) recorded in ZG cells from Calbryte 520 AM-stained adrenal slices over 7.5 min is lower in WT than in KO (WT, blue: $n_{animals}$ = 7, n_{slices} = 11, n_{cells} = 208; KO, orange: $n_{animals}$ = 5, n_{slices} = 7, n_{cells} = 103; P=0.0026; likelihood ratio test of linear mixed models). Individual larger colored and smaller grey spots represent mean values per slice and cell, respectively. The mean of all mean values per slice are shown as white circles ± 95% confidence interval (error bars, CI).* ***(D-E)*** *Mean $[Ca^{2+}]_{int}$ in ZG cells as determined by imaging of adrenal slices stained with Fura-2 AM. The Ang II concentration was kept constant at 100 pmol/l in* ***(D)*** *while potassium was fixed at 4 mmol/l in* ***(E)****. Data in D and E are plotted as mean values of all cells (circles) ± 95% CI (shaded areas). See Supplementary Tables S1, S2 and S3 for statistical information of data in C, D and E, respectively. Confidence intervals were calculated from a bootstrap resampling.*

ZG stimulation results in similar changes of intracellular calcium levels in KO and WT mice

The higher activity may represent a compensatory mechanism in KO cells to reach mean $[Ca^{2+}]_{int}$ similar to WT cells. We therefore investigated mean $[Ca^{2+}]_{int}$ over a wide range of concentrations of potassium (Fig. 1D) and Ang II (Fig. 1E). With increasing stimulation, $[Ca^{2+}]_{int}$ similarly increased in ZG cells of both, WT and KO. Mean $[Ca^{2+}]_{int}$ were not significantly different between genotypes (Supplementary Tables S2 and S3), suggesting that the higher activity and intra-burst frequency of calcium spikes in KO cells does not result in higher calcium influx over time but rather maintains the sensitivity to physiological stimuli of aldosterone production.

Bulk RNA-seq of adrenal cortices from KO mice revealed no upregulation of calcium transport genes

To identify up- or downregulated transcription of genes in response to the loss of $Ca_V3.2$ and to quantify the expression of voltage-gated calcium channels in WT, we performed bulk RNA-sequencing of adrenal cortices from 6 WT and 5 KO mice.

In WT, *Cacna1h* ($Ca_V3.2$), *Cacna1c* ($Ca_V1.2$) and *Cacna1d* ($Ca_V1.3$) (Fig. 2A, Supplementary Table S4) were the most strongly expressed voltage-gated calcium channel α1-subunit genes. The most prominent channel subunits were β2 and α2δ1 (Supplementary Table S4).

Apart from a downregulation of *Cacna1h* mRNA, likely due to nonsense-mediated decay, we did not observe any significant changes to known calcium channel genes in KO (other than *Cacna1h*) compared to WT mice (Supplementary Table S4). In total, we observed 12 differentially expressed genes with at least a 2-fold change between genotypes (Fig. 2B and 2C, Supplementary Table S5). Of these, besides *Cacna1h*, only *Creb5* has previously been associated with regulating aldosterone synthesis[23].

Looking at other known genes involved in aldosterone synthesis (according to the KEGG database) without cutoff for the change in expression, there was only a small but significant upregulation of the type 1a angiotensin receptor (1.35-fold, $p_{adj} = 0.048$) and *Star* (1.27-fold, $p_{adj} = 0.007$), as well as a downregulation of *Gna11* (0.87-fold, padj = 0.023) in KO adrenal cortices (Supplementary Table S6).

We additionally conducted GO term and KEGG pathway overrepresentation analyses for the set of differentially expressed genes but did not observe any over- or under-represented terms or pathways including for aldosterone synthesis in general.

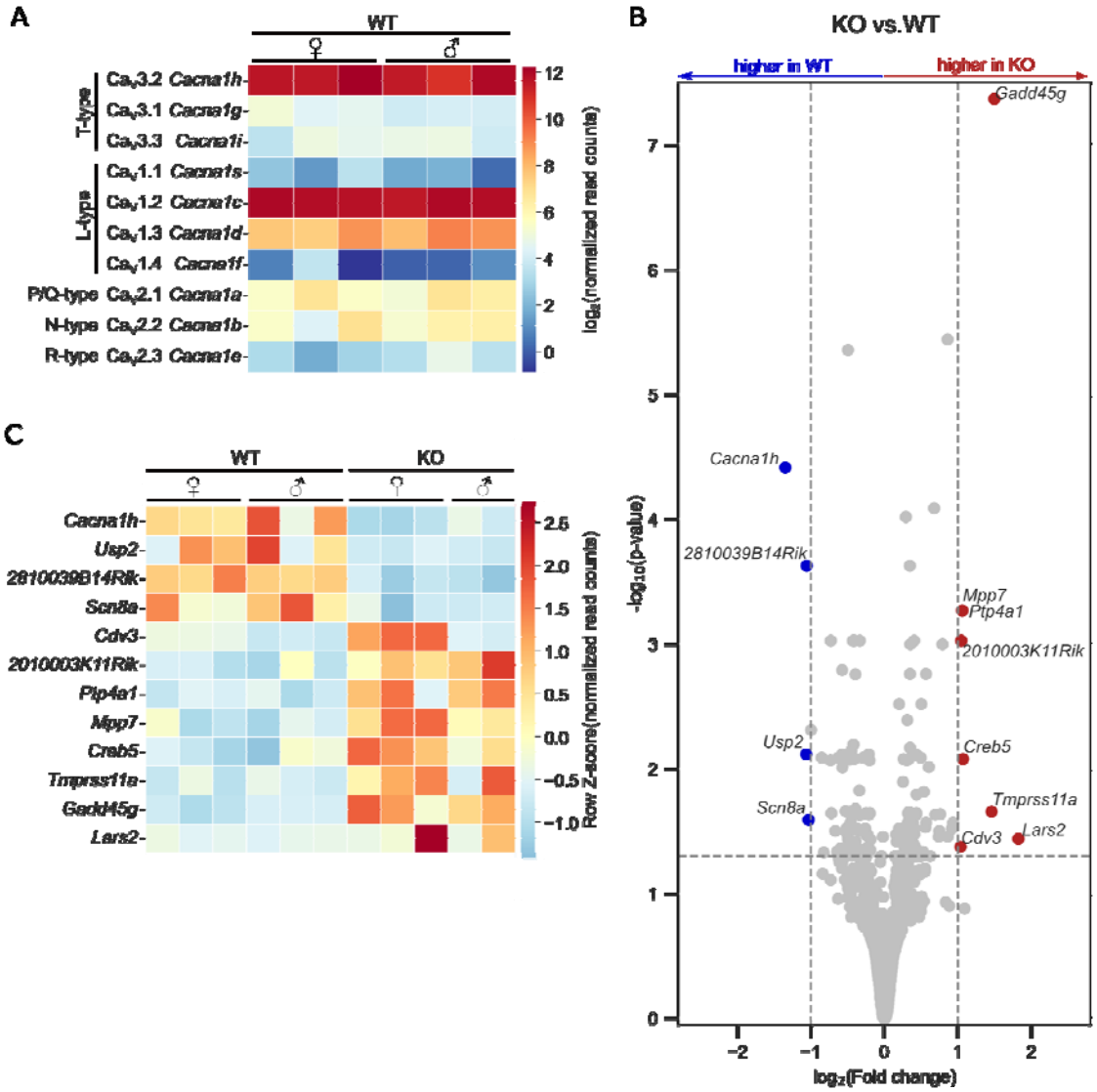

Figure 2. RNA-seq reveals only few differentially expressed genes.

(A) *Heat map illustrating the normalized log_2 transformed read counts of voltage-gated calcium channel transcripts detected in WT samples (columns, $n_{animals,WT}$ = 6).* ***(B)*** *Volcano plots with the log_2-fold change (LFC, cutoff = |1|) in gene expression in KO vs. WT samples ($n_{animals,WT}$ = 6, $n_{animals,KO}$ = 5) and the log_{10} transformed statistical significance (p-value, corrected for multiple testing, transformed cutoff=0.05). The 12 differentially expressed genes (DEGs) with more than 2-fold change are highlighted as up- (red) or down (blue) regulated.* ***(C)*** *Heatmap illustrating the row Z-score of the normalized read counts of significantly up- or down regulated genes sorted by their LFC.*

Adrenocortical cells from KO mice do not exhibit T-type calcium currents

To investigate the functional contribution of the calcium conductances present in the adrenal cortex of KO and WT and to confirm the functional loss of $Ca_V3.2$ in our KO mice, we performed whole cell patch clamp recordings from isolated adrenocortical cells. Currents were recorded in response to two separate voltage clamp protocols[24] (Supplementary Fig. S2): First from a holding potential of -80 mV, then from a holding potential of -40 mV. At -80 mV, voltage-gated calcium channels reside in the closed but activatable state leading to currents from all types of calcium channels (Supplementary Fig. S2, left). With the second protocol (from -40 mV), the low-voltage activated T-type channels are already inactivated before the recording. Only non-T-type calcium channels (including the L-type channels $Ca_V1.2$ and $Ca_V1.3$) remain available (Supplementary Fig S2, middle). The subtraction of the current from the holding potential of -40 mV from the one from -80 mV revealed the T-type channel component (Supplementary Fig. S2, right). In WT cells, we observed both, T- and non-T-type currents in all recorded cells (7 cells from 3 animals, Fig. 3A-B). In KO cells, we did not observe T-type currents in any of the recorded KO cells (9 cells from 4 animals, Fig. 3A). Non-T-type currents observed in KO cells were not different in their maximum amplitude or voltage dependence compared to WT cells (Fig. 3B). This excludes large post-translational modifications to increase L-type currents in response to the loss of $Ca_V3.2$.

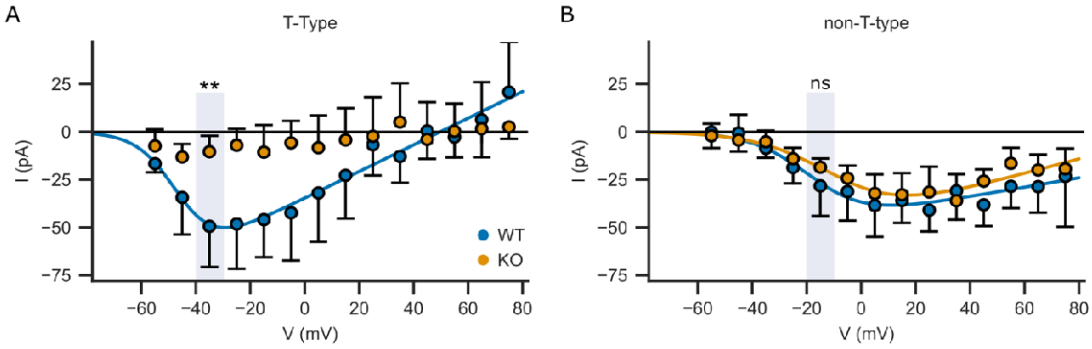

Figure 3. ZG cells from KO cells lack T-type currents. *Whole cell patch-clamp recordings were performed in isolated adrenocortical cells from WT and KO mice.* ***(A)*** *Voltage dependence of the T-type peak current amplitudes expressed as I-V curves. Comparison at -35 mV: p= 0.003 (WT: $n_{animals}$ = 3, n_{cells} = 7; KO: $n_{animals}$ = 4, n_{cells} = 9, likelihood ratio test of linear mixed models).* ***(B)*** *Voltage dependence of the non-T-type peak current amplitudes. Comparison at -15 mV: p=0.676 (WT: $n_{animals}$ = 3, n_{cells} = 7; KO: $n_{animals}$ = 4, n_{cells} = 9, likelihood ratio test of linear mixed models). Data in A and B are*

shown as mean + or - 95% CI. Solid lines represent fits of the experimental data by equation 1. For clarity, only one half of the CI is displayed.

$Ca_V3.2$ is not required for calcium oscillations in WT mice

The lack of observable T-type currents already suggested that $Ca_V3.2$ was the only relevant T-type calcium channel in adrenocortical cells. To further confirm its importance for calcium oscillations specifically in the ZG, we studied the effect of the T-type calcium channel inhibitor TTA-P2[25] in adrenal slice preparations of KO and WT using calcium imaging. We used TTA-P2 at a concentration of 15 µmol/l, slightly higher than what was used previously in ZG cells[10]. At this concentration, virtually all T-type calcium channels are expected to be inhibited but less than 10 % of L-type channels[26].

ZG cells from KO mice showed unchanged oscillatory calcium changes in the presence of TTA-P2 (Fig. 4A), further suggesting the absence of other T-type channels. Treatment of WT slices led to a heterogeneous response, with some cells exhibiting continued calcium spiking (Fig. 4B) and others turning completely silent (Fig. 4C). Overall, only ~34% of the WT cells remained active while KO cells remained almost unaffected (WT: 34.4%, 95% CI: 22.2-47.3%; KO: 90.3%, 95% CI: 84.3-95.1%; Fig. 4D).

This resulted in a reduction of the mean activity in WT but not in KO cells when compared to control recordings (Fig. 4E and F; absolute data in Supplementary Fig. S3A).

WT cells with remaining activity in the presence of TTA-P2 showed an increased intra-burst frequency relative to untreated controls but stayed below the level of KO (Fig. 4G; absolute data in Supplementary Fig. S3B, C).

These findings support an important role of $Ca_V3.2$ also in the generation of calcium spikes in WT mice. Still, at least in some cells, other calcium influx pathways exist that can maintain calcium oscillations in the absence of T-type calcium channels.

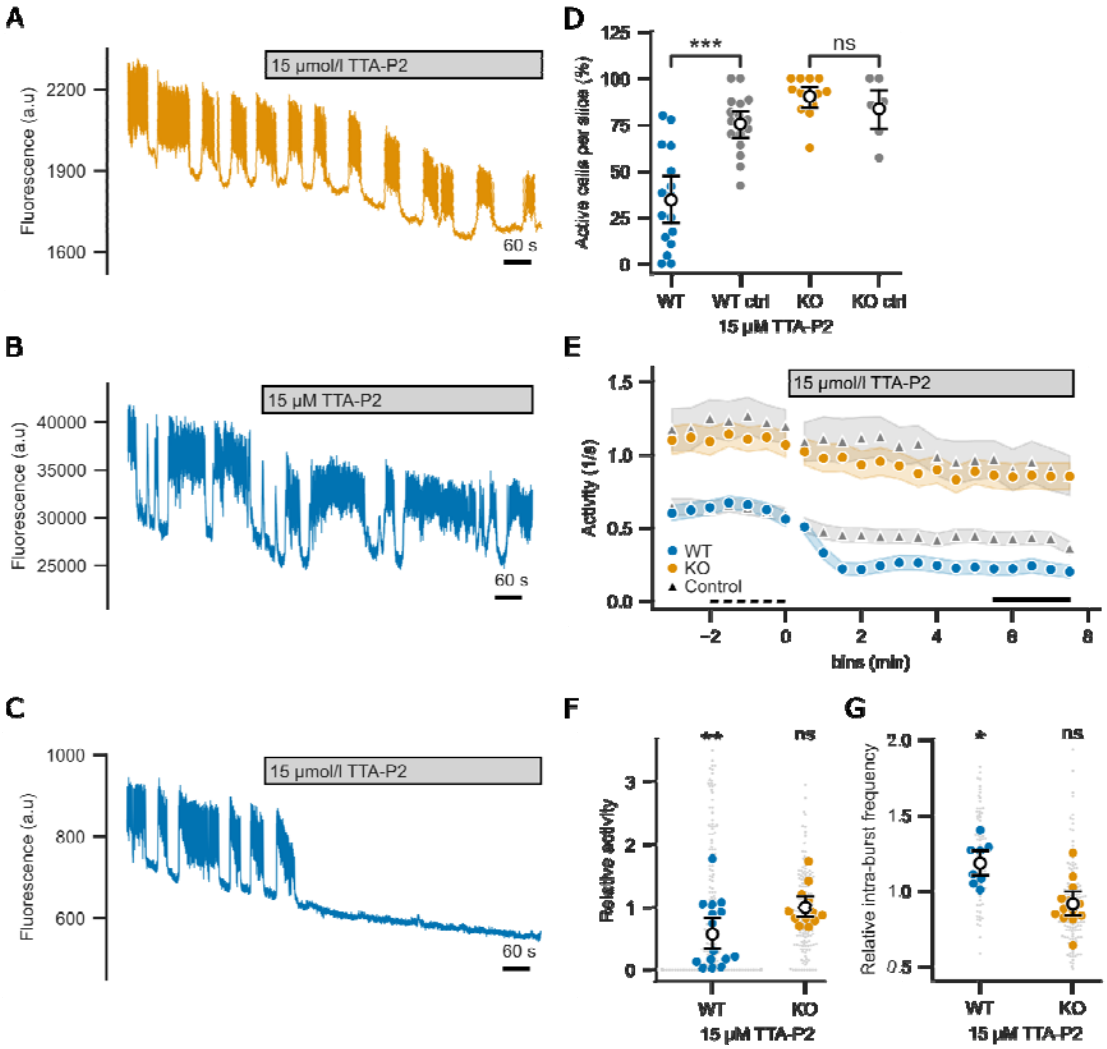

Figure 4. TTA-P2 only partially inhibits calcium oscillations in ZG cells of WT mice. (A-C) *Variations in the fluorescence recorded in one representative KO* ***(A)*** *and two WT* ***(B-C)*** *ZG cells from adrenal slices stained with Calbryte 520 AM at 4 mmol/l K^+ and 500 pmol/l Ang II. Application of TTA-P2 (15 µmol/l, indicated by the grey bar) inhibits calcium spikes in a fraction of the WT cells.* ***(D)*** *Fraction of cells in a slice that are still active under 15 µmol/l TTA-P2 (determined at time span 5.5 - 7.5 minutes after addition of TTA-P2, indicated by the black line in D) compared to the number of active cells before application of TTA-P2 (-2 - 0 minutes, i.e., baseline, indicated by the black dashed line in D). This value was significantly lowered in WT slices but not KO slices compared to respective controls.* ***(E)*** *In WT (blue) but not KO (orange) ZG cells from Calbryte 520 AM-stained adrenal slices, calcium spike activity (in 0.5 minutes bins) was lowered by 15 µmol/l TTA-P2 (circles: mean; colored area: 95% CI) when compared to controls (no TTA-P2, triangles: mean; grey area: 95% CI).* ***(F)*** *Relative activity between 5.5 – 7.5 minutes after the start of the perfusion was significantly changed by 15 µmol/l TTA-P2 in WT but not KO.* ***(G)*** *Relative intra-burst frequency was significantly changed by 15 µmol/l TTA-P2 in WT but not KO. Individual values per slice and cell are shown as larger and smaller circles, respectively.*

*Overall mean values over slices in E-G are expressed in mean (white circles) ± 95% CI (error bars; WT: $n_{animals}$ = 10, n_{slices} = 16, n_{cells} = 291; KO: $n_{animals}$ = 7, n_{slices} = 13, n_{cells} = 162; WT control: $n_{animals}$ = 15, n_{slices} = 17, n_{cells} = 288; KO control: $n_{animals}$ = 7, n_{slices} = 7, n_{cells} = 83). Data in E and G was calculated relative to control recordings. Values per genotype were tested against respective controls (likelihood ratio test of linear mixed models). P values are indicated as follows: ns, P ≥ 0.05; *P < 0.05; **P < 0.01; ***P < 0.001. See Supplementary Tables S7-S11 for statistical information and Supplementary Figure S3 for absolute values of F and G.*

L-Type calcium channels mediate calcium oscillations in KO mice

Besides T-type channels, our RNA-seq data also demonstrated the expression of L- and, to a lesser extent, N- and P/Q-type calcium channels in the adrenal cortex. To test for the contribution of L-type channels to calcium signaling in the ZG of WT and KO mice, we perfused adrenal slices with the specific L-type channel inhibitor isradipine and performed calcium imaging.

The concentration of isradipine was chosen to be rather specific for L-type calcium channels[27–30]. We applied a concentration of 0.05 µmol/l, which may not completely inhibit $Ca_V1.3$ (only to ~70%[27]). The onset of inhibition was slow but resulted in an almost complete termination of calcium signaling in KO cells but nearly no effect in WT cells (Fig. 5A-C). Calcium spiking was almost completely attenuated in KO without significant effect on WT compared to controls (Fig. 5C and D; absolute data in Supplementary Fig. S4A). Isolated bursts, however, still occurred, resulting in a significant decrease of active cells in KO mice to ~32% (31.8%, 95% CI: 23.8-42.1%) after 5.5 to 7.5 minutes after the onset of perfusion (Fig. 5E). In contrast, almost all WT cells were still active in the same time frame (Fig. 5E).

The intra-burst frequency remained unaffected by the inhibition of L-type channels in both genotypes (Fig. S4B-C).

Overall, these results indicate that L-type calcium channels are essential to generate the activity in mice lacking $Ca_V3.2$. However, acute inhibition of L-type channels alone did not significantly change the calcium spiking in WT ZG cells.

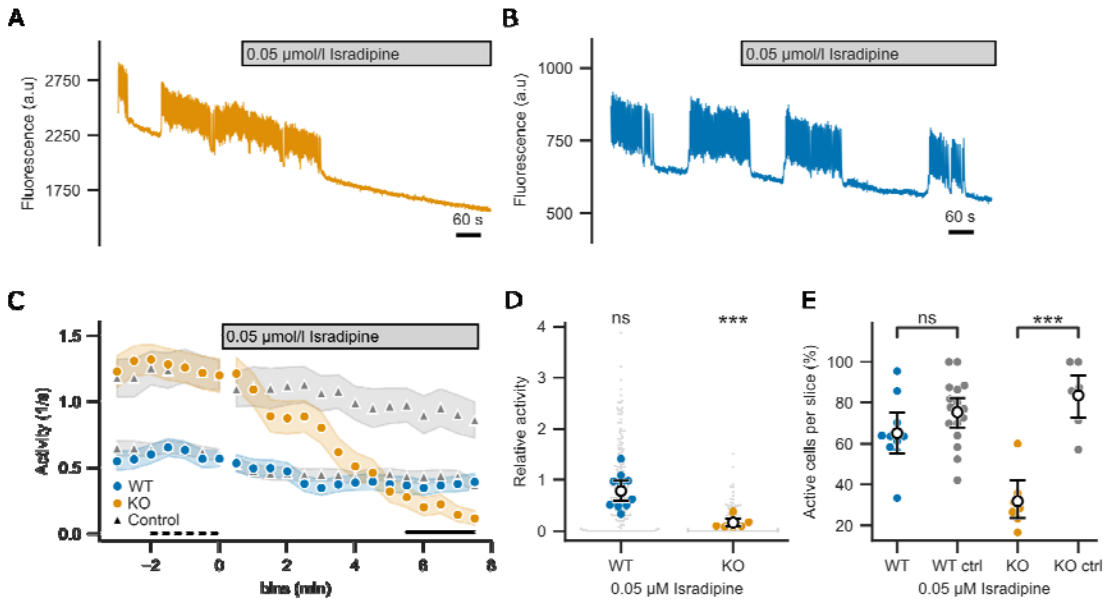

Figure 5. The L-type inhibitor isradipine inhibits calcium oscillations in KO but not WT cells. (A-B) *Variations in the fluorescence recorded in one representative KO* ***(A)*** *and WT* ***(B)*** *ZG cell from adrenal slices stained with Calbryte 520 AM at 4 mmol/l K^+ and 500 pmol/l Ang II. Application of isradipine (0.05 µmol/l, indicated by the grey bar) inhibits calcium spikes in almost all KO but not WT cells.* ***(C)*** *Calcium spike activity (in 0.5 minutes bins) of ZG cells from KO (orange) but not WT (blue) Calbryte 520 AM-stained adrenal slices, was lowered by 0.05 µmol/l isradipine (mean: circle; colored area: 95% CI).*

(D) *Calcium spike activity (relative to control) was significantly changed by isradipine in KO but not WT.* ***(E)*** *Fraction of cells in a slice that are still active at 0.05 µmol/l isradipine (time span 5.5 - 7.5 minutes after addition of isradipine, indicated by the black line in C) compared to cells at zero isradipine (-2 - 0 minutes, i.e., baseline, indicated by the black dashed line in C) was significantly lowered in KO but not WT when compared to control. Individual values per slice and cell are shown as larger and smaller circles, respectively. Overall mean values per genotype are shown in D-E as white circles ± 95% CI (error bars; WT: $n_{animals} = 9$, $n_{slices} = 10$, $n_{cells} = 178$; KO: $n_{animals} = 6$, $n_{slices} = 7$, $n_{cells} = 107$; WT control: $n_{animals} = 15$ $n_{slices} = 17$, $n_{cells} = 288$; KO control: $n_{animals} = 7$, $n_{slices} = 7$, $n_{cells} = 83$). Data in D was calculated relative to control recordings. Values per genotype were tested against respective controls (likelihood ratio test of linear mixed models). P values are indicated as follows: ns, $P \geq 0.05$; ***$P < 0.001$. See Supplementary Tables S12-S16 for statistical information and Supplementary Figure S4 for absolute values of D.*

Both, T- and L-type calcium channels are needed for Ang II-dependent calcium signaling

To test whether other (non T- nor L-type) calcium channels contribute to the generation of $[Ca^{2+}]_{int}$ oscillations in WT, we studied the situation in ZG cells upon inhibition using both, TTA-P2 and isradipine. The protocol consisted of a 10-minute period in which the slice was perfused with the T-type calcium channel inhibitor TTA-P2 alone, followed by another 10 minutes during which TTA-P2 was supplemented with isradipine to additionally block L-type calcium channels. To maximize the specificity of the inhibition of T- over L-type channels, we lowered the concentration of TTA-P2 to 5 µmol/l. Furthermore, we increased the isradipine concentration to 300 nmol/l to fully inhibit $Ca_V1.3$[27]. A potential unspecific inhibition of T-type channels was considered less important in this context given the parallel incubation with TTA-P2. (Fig. 6A, B).

As observed for the higher concentration (Fig. 4D-G), TTA-P2 alone only incompletely reduced the activity (Fig. 6B-C; absolute data in Supplementary Fig. S5A) and the number of active cells (Fig. 6D) but increased the intra-burst frequency (Fig. 6E; absolute data in Supplementary Fig. S5B). Addition of isradipine led to a cessation of all signals, demonstrating that the combination of both, T- and L-type calcium channels, is necessary for calcium oscillations and cannot be substituted for by other calcium channels.

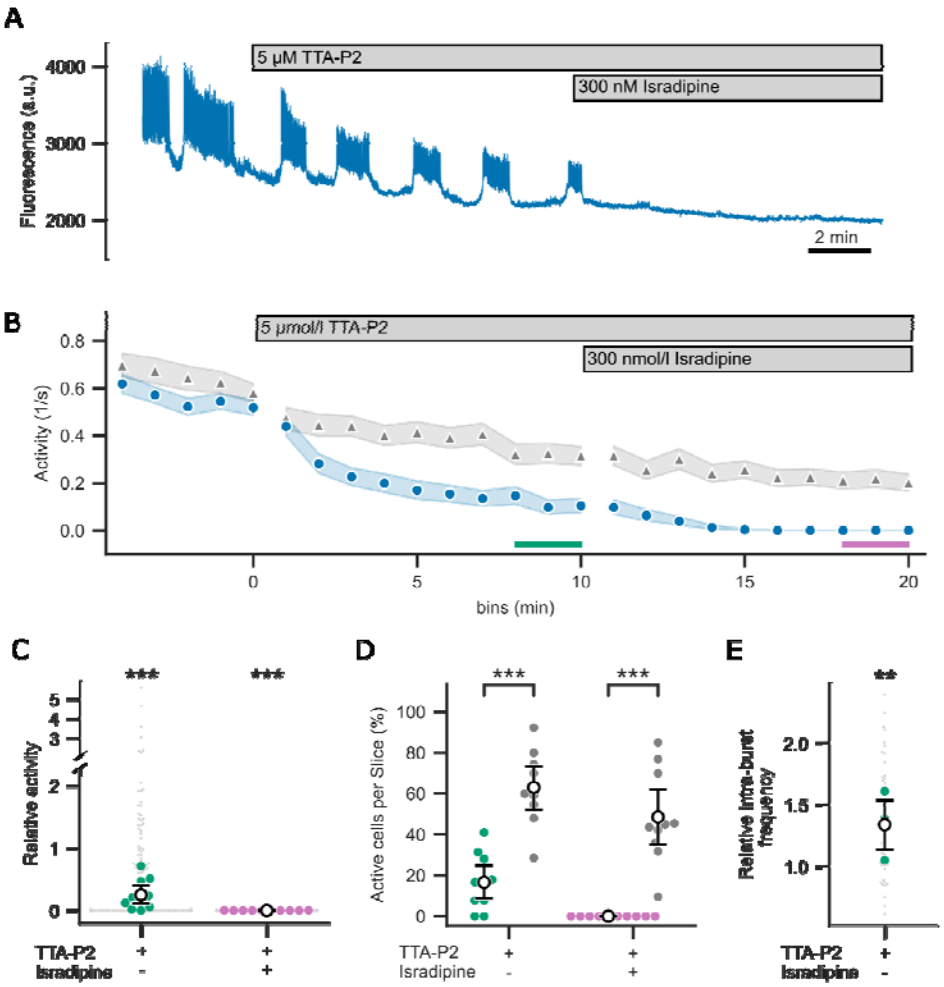

Figure 6. Simultaneous inhibition of L- and T-type calcium channels fully abolishes calcium signaling. (A) *Fluorescence intensity recorded from one representative WT ZG cell from an adrenal slice stained with Calbryte 520 AM at 4 mmol/l K^+ and 500 pmol/l Ang II. Simultaneous application of TTA-P2 (5 µmol/l) and isradipine (0.3 µmol/l, indicated by grey bars) abolishes calcium spikes.* ***(B)*** *Calcium spike activity (in 1-minute bins) of WT ZG cells from Calbryte 520 AM-stained adrenal slices was lowered by 5 µmol/l TTA-P2 and 300 nmol/l isradipine at 4 mmol/l K^+ and 500 pmol/l Ang II compared to control (mean: blue circle; colored area: 95% CI). Activity of control cells (no blockers) is shown as grey triangles (mean circles ± 95% CI, grey areas). The last two minutes of each condition comprising inhibitors (steady-state phase) of the recording are highlighted with color-coded lines. (WT: $n_{animals}$ = 6, n_{slices} = 10, n_{cells} = 246; WT control: $n_{animals}$ = 9, n_{slices} = 10, n_{cells} = 213).* ***(C)*** *Calcium activity in ZG cells from WT adrenal slices during the steady-state phases as highlighted in B.* ***(D)*** *Fraction of cells in a WT adrenal slice that were active during the steady-state phases as indicated in B compared to untreated controls (grey).* ***(E)*** *Intra-burst frequency of WT cells during the green steady-state phase as indicated in B relative to controls. Mean values in for each cell are shown in C and E as smaller grey circles. Mean values for each slice are shown as larger (colored or grey) circles*

*and overall means per group are shown as white circles ± 95% CI (C-E). Values per group were tested against WT controls (likelihood ratio test of linear mixed models). P values are indicated as follows: **P < 0.01; ***P < 0.001. See Supplementary Tables S17-S21 for statistical information and Supplementary Figure S5 for absolute values of C and E.*

Only T- and L-type calcium channels contribute to the Ang II-dependent calcium influx in the murine ZG

Our investigations so far only considered oscillatory calcium changes in response to stimulation with Ang II. Other calcium sources such as intracellular stores or other calcium channels may however mediate non-oscillatory increases of $[Ca^{2+}]_{int}$. To test this hypothesis, we determined mean and baseline $[Ca^{2+}]_{int}$, i.e. $[Ca^{2+}]_{int}$ during pauses or in the absence of spiking, over time. In the absence of Ang II, almost no spikes could be observed, and mean and baseline $[Ca^{2+}]_{int}$ were indistinguishable (Fig. 7A-C). When extracellular Ang II was increased to 100 pmol/l, cells with oscillatory activity could be identified. This resulted in an increase of mean $[Ca^{2+}]_{int}$ over baseline values. $[Ca^{2+}]_{int}$ oscillations were subsequently inhibited by perfusion with a combination of 5 µmol/l TTA-P2 and 300 nmol/l isradipine for 10 minutes (Fig. 7B-C; Supplementary Fig. S6) as before. This resulted in mean $[Ca^{2+}]_{int}$ decreasing to values close to those prior to stimulation with Ang II and also attenuated the small increase in baseline $[Ca^{2+}]_{int}$ before inhibition (Fig. 7C-D). A further increase of Ang II to 500 pmol/l did not raise $[Ca^{2+}]_{int}$ when T- and L-type calcium channels were inhibited (Fig. 7B-C).

Our results show that increases of $[Ca^{2+}]_{int}$ are only caused by the oscillatory influx of calcium through T-type ($Ca_V3.2$) and L-type ($Ca_V1.2$/$Ca_V1.3$) calcium channels. Other sources including other calcium channels or intracellular stores do not contribute.

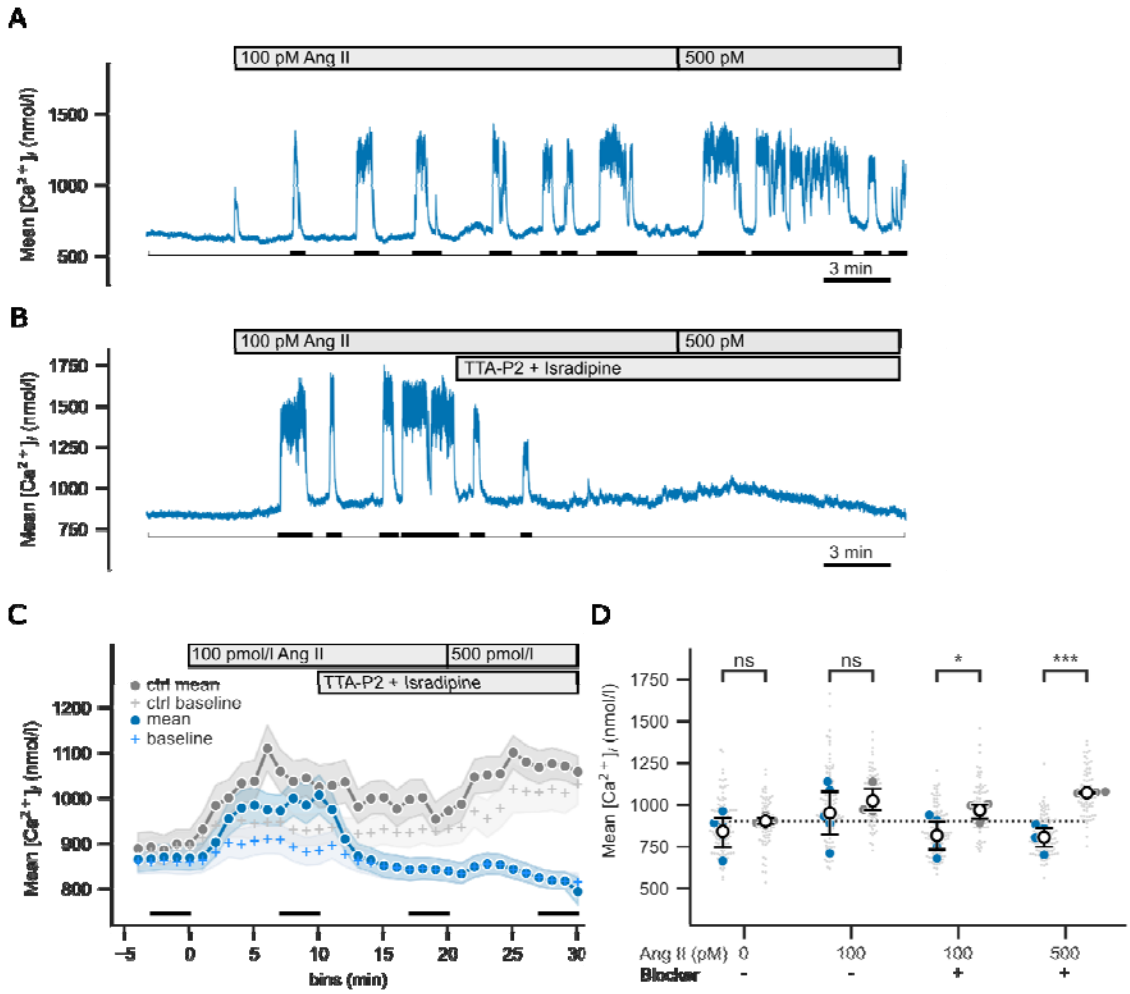

Figure 7. T- and L-type channels mediate Ang II evoked calcium oscillations

(A) *Representative trace of intracellular calcium concentrations of a ZG WT cell from a Fura-2-AM-stained adrenal slice at varying concentrations of Ang II without inhibitors (control).* ***(B)*** *Representative trace of intracellular calcium concentrations of a ZG WT cell from a Fura-2-AM-stained adrenal slice before and during perfusion with inhibitors TTA-P2 (5 µmol/l) and isradipine (300 nmol/l) at varying concentrations of Ang II. Empty and filled bars in A and B indicate baseline and burst phases, respectively.* ***(C)*** *Mean intracellular calcium concentrations (circles; ± 95% CI are shown as shaded areas) at 4 mmol/l K^+ of cells from adrenal slices stained with Fura-2-AM. Ang II-stimulated increase in $[Ca^{2+}]_i$ was abolished by 5 µmol/l TTA-P2 and 300 nmol/l isradipine, and increasing Ang II concentration did not result in any increase of intracellular calcium concentration in the presence of blockers (blue). Corresponding control is shown in grey (circles, no perfusion of blockers). Mean intracellular calcium concentrations during baseline phases are indicated by crosses (light blue: treated, light grey: untreated control).* ***(D)*** *Mean intracellular calcium concentrations of ZG cells from Fura-2-AM-stained adrenal slices before and during perfusion with both inhibitors TTA-P2 (5 µmol/l) and isradipine (300 nmol/l) at varying concentrations of Ang II as indicated in C (black bars, grey*

*circles: untreated controls). Mean values for each slice and cell are shown as blue and grey circles, respectively. Overall means per group are shown as white circles ± 95% CI (WT: $n_{animals}$ = 5, n_{slices} = 5, n_{cells} = 117; WT control: $n_{animals}$ = 3, n_{slices} = 4, n_{cells} = 69). See Supplementary Tables S22 and S24 for statistical information. P values are indicated as follows: ns, P ≥ 0.05; *P < 0.05; ***P < 0.001.*

L-type calcium channels are expressed in all ZG cells

The heterogeneous nature of the effects of TTA-P2 and isradipine led us to investigate whether differences in the expression of the main L- and T-type voltage gated calcium channels exist in the ZG. For this, we obtained access to a single-nuclear RNA-seq data set of mouse adrenal glands (unpublished data by AKS and UIS). We selected ZG cells based on the expression of *Dab2*, *Cacnb2*, *Agtr1b* and *Agtr1a* (see methods). Plotting the normalized, natural-log transformed counts of transcripts for the T-type channel $Ca_V3.2$/*Cacna1h* versus the L-type channel $Ca_V1.3$/*Cacna1d* reveals four subsets of cells (Fig. 8A). The first consists of cells without detected RNA transcripts for either channel (red 1: 2252/6589 cells; 34%). There are also subsets of cells without detected *Cacna1d* but with *Cacna1h* transcripts (red 2: 1353 cells; 21%) and cells expressing *Cacna1d* without detected *Cacna1h* (red 3: 1729 cells; 26%). A similar number of cells expressed both, *Cacna1d* and *Cacna1h* (red 4: 1255 cells; 19%). In general, the absolute count of transcripts of either of these two channels per cell was very low (less than 5). In contrast, almost all ZG cells exhibit expression of $Ca_V1.2$/*Cacna1c* (Fig. 8B and C; 8 cells without detected *Cacna1c* transcripts). Raw counts were higher by an order of magnitude compared to the other two channels. We conclude that virtually all cells of the ZG express the L-type channel $Ca_V1.2$, while $Ca_V1.3$ and $Ca_V3.2$ are less abundantly found.

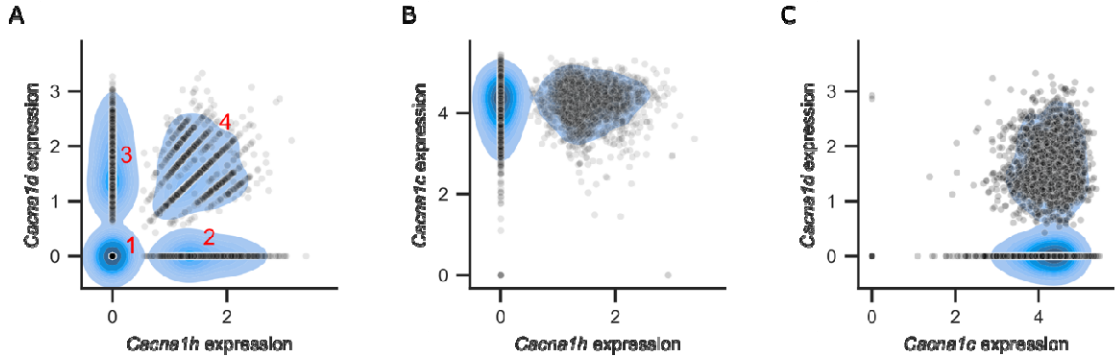

Figure 8. All ZG cells have transcripts for $Ca_V1.2$ but not necessarily $Ca_V1.3$ or $Ca_V3.2$

(A) *Plot of the normalized, natural-log transformed counts of Cacna1d ($Ca_V1.3$) versus Cacna1h ($Ca_V3.2$) as individual points per cell. A kernel density plot of the data is plotted below in blue with darker color indicating higher density of values underneath. Red numbers indicate expression clusters explained in the text. The striped appearance in cluster 4 is due to the low number of Cacna1h and Cacna1d counts.* ***(B)*** *Plot of the normalized, natural-log transformed counts of Cacna1c ($Ca_V1.2$) versus Cacna1h ($Ca_V3.2$) as in (A).* ***(C)*** *Plot of the normalized, natural-log transformed counts of Cacna1c ($Ca_V1.2$) versus Cacna1d ($Ca_V1.3$) as in (A).*

Discussion

The zona glomerulosa is a complex system with several stimuli regulating the synthesis of aldosterone[4]. It has long been postulated that most of these factors, including serum potassium and Ang II, act by mediating oscillatory calcium influx into ZG cells elicited through depolarization of the cell membrane[4] and also through release of calcium from intracellular stores[7,8]. The depolarizations were previously reported to be dependent on T-type calcium channels, in particular $Ca_V3.2$.

In this manuscript, we demonstrate that:

1) Ang II and potassium dependent $[Ca^{2+}]_{int}$ oscillations still occur in $Ca_V3.2$ knock out mice and are instead dependent on L-type calcium channels.

2) Acute inhibition of T-type calcium channels does not abolish Ang II dependent calcium influx into the wild-type ZG. Rather, a subset of cells still demonstrates oscillatory calcium influx via L-type calcium channels.

3) Ang II (and potassium) increase $[Ca^{2+}]_{int}$ in ZG cells only via T- and L-type calcium channels with no support from intracellular calcium stores.

Hu et al. demonstrated that murine ZG cells constitute electrical oscillators with action potential-like depolarizations that were critically dependent on the voltage-gated T-type calcium channel $Ca_V3.2$[15]. It is likely that these voltage oscillations are the basis of ZG calcium oscillations as they exhibit similar frequencies and stimulus dependence (Fig. 1)[9–11]. However, while likely linked, it is not the change in voltage itself but ultimately the influx of calcium that is required for the physiological function of the ZG. Contrary to what would be expected if $Ca_V3.2$ was solely necessary for maintaining calcium signaling, knock-out mice did not show reduced aldosterone levels[11,22]. However, these studies investigated KO mice on a systemic level, and secondary mechanisms (such as activation of the renin-angiotensin system or upregulation of other calcium influx pathways in the ZG) may have compensated for the loss. We therefore investigated the mechanisms regulating calcium influx in the ZG of mice lacking the $Ca_V3.2$ channel in comparison to WT mice in acute slice preparations and isolated adrenocortical cells.

We found that calcium signaling was largely unaffected by the loss of $Ca_V3.2$ in KO mice (Fig. 1). Despite a slight increase in the spiking activity, mean levels of $[Ca^{2+}]_{int}$ in the ZG were

indistinguishable from WT, explaining why aldosterone levels were unchanged (Fig. 1D and E).

It was suggested that other T-type channels, which may compensate for the loss of $Ca_V3.2$, may also be important for aldosterone synthesis[22]. However, our data from RNA-seq (Fig. 2A) did not suggest relevant expression of T-type channels other than *Cacna1h* in the adrenal cortex. Adrenocortical cells from KO mice lacked T-type currents (Fig. 3). Furthermore, perfusion of slices from adrenals of KO mice with the T-type inhibitor TTA-P2 did not result in changes to calcium signaling (Fig. 4), supporting that $Ca_V3.2$ is indeed the only relevant T-type voltage-gated calcium channel in the ZG.

On the other hand, perfusion with the L-type calcium channel inhibitor isradipine almost completely suppressed $[Ca^{2+}]_{int}$ oscillations in KO mice (Fig. 5), demonstrating that these signals instead depend on L-type calcium channels. Based on previous knowledge[15,17,19,21] and our bulk RNA-seq analysis (Fig. 2A), the L-type calcium channels most prominently expressed in the murine and human adrenal cortex are $Ca_V1.3$ and $Ca_V1.2$[15,17,19]. We did not find evidence of compensatory upregulation of L-type or any other calcium channels or transporters in KO mice. Patch clamp experiments also ruled out large post-translational changes to voltage-gated calcium channels as current amplitudes were similar in WT and KO mice (Fig. 3).

The importance of L-type channels had already been previously demonstrated by studies identifying somatic gain-of-function $Ca_V1.3$ mutations in patients with primary aldosteronism [17,21,31–33]. Furthermore, there are previous reports that aldosterone synthesis in human ZG is dependent on both, T- and L-type, calcium channels[19,34]. It is currently not known whether human ZG cells exhibit similar voltage and $[Ca^{2+}]_{int}$ oscillations as murine ones. However, species differences in the ion channels involved seem to be mainly in the composition of potassium channels[35], while the expression of calcium channels is rather similar[17,19,35,36].

Currently, we cannot explain why $[Ca^{2+}]_{int}$ oscillations were faster in KO than in WT mice. The mechanisms behind initiation and termination of oscillations beyond $Ca_V3.2$ and background potassium channels are still insufficiently understood. It had already been suggested that additional conductances must underlie the initial depolarization in WT[15], and this is confirmed by our results, as L-type channels ($Ca_V1.3$ and even more so 1.2) require even stronger depolarization for activation and are unlikely to drive depolarization from a

potassium-defined resting membrane potential on their own. Clearly, the closure of TASK potassium channels is involved in permitting (Ang II-dependent) depolarization[5,6,37], but still other conductances must mediate the initial depolarization itself.

Also, it is currently unclear how individual spikes and bursts are terminated. We previously observed slower spiking in a gain-of-function *Cacna1h* knock-in model. Given that the knock-out presented here should generally lead to the opposite effect, it is a tempting speculation that the frequency of calcium spiking is inversely linked to intracellular [Ca^{2+}]. In our knock-out model this would serve to sustain physiological calcium levels (and hence aldosterone synthesis). Previous observations have suggested a role for calcium-dependent potassium channels[20,38] in the ZG, which may control spiking, but further work is necessary to understand their functional importance. This would best combine *in situ* electrophysiological studies with simultaneous calcium imaging, which we were unfortunately unable to perform here.

Besides the situation of a chronic loss of $Ca_V3.2$ as in our knock-out model, our data also imply that physiological calcium signaling in the ZG is not solely dependent on $Ca_V3.2$. Acute inhibition of T-type voltage gated calcium channels with the specific blocker TTA-P2 in WT mice only attenuated activity by approximately 50-20 % (Fig. 4&6). $[Ca^{2+}]_{int}$ oscillations could only be completely inhibited when simultaneously blocking L-type calcium channels using isradipine (Fig. 6). Acute inhibition of L-type channels in isolation, however, did not alter calcium spiking (Fig. 5). This suggests that the generation of oscillations in WT ZG cells is primarily dependent on $Ca_V3.2$. However, following the acute inhibition of T-type calcium channels, for example via TTA-P2, L-type channels can maintain some degree of calcium signaling in WT cells (Fig. 4). Cells with remaining activity after inhibition of $Ca_V3.2$ exhibited higher intra-burst frequencies than before inhibition (Fig. 4G; Supplementary Fig. S3B), suggesting that a similar mechanism as in KO cells is also present in a subset of WT cells.

Our analysis of murine single-nuclear RNA-seq data suggests that $Ca_V1.2$ is expressed in all ZG cells while transcripts for $Ca_V1.3$ were not found in all ZG cells (Fig. 8). The latter could be due to lower expression levels and low sensitivity of single-nuclear sequencing. It remains puzzling why no L-type currents were observed in ZG cells in the study by Hu et al., even when stimulated with the L-type channel activator Bay K8644[15]. In contrast, we observed L-type currents in all cells recorded using whole cell patch-clamp, even without further

stimulation (Fig. 3). While this discrepancy might be explained by the difference in cell preparation (in-situ patch clamp[15] versus dissociated adrenocortical cells in our study), our calcium imaging experiments and results from single-nuclear RNA-seq (Fig. 8) also clearly support the relevance of L-type calcium channels in generating and maintaining calcium oscillations in the ZG of both genotypes, WT and KO, *in situ*.

Furthermore, we could demonstrate that Ang II mostly changes $[Ca^{2+}]_{int}$ through variations of the patterns of oscillations and not by altering baseline levels (Fig. 7C). Simultaneous inhibition of T- and L-type calcium channels not only completely stopped Ang II dependent $[Ca^{2+}]_{int}$ oscillations but also any changes in baseline $[Ca^{2+}]_{int}$. This excludes a role for other calcium influx pathways besides voltage-gated calcium channels in the control of aldosterone synthesis by Ang II. While we did not test whether stimulation of aldosterone synthesis with K^+ is similarly dependent on voltage-gated calcium channels, the observation that a response to physiological changes of K^+ only occurs in the presence of Ang II[9,10] makes this a plausible assumption. However, it should be noted that, even after inhibition of T- and L-type calcium channels, baseline $[Ca^{2+}]$ remained high compared to most other cell types. We have observed that baseline calcium can be lowered by the removal of extracellular calcium (unpublished observation by HAD and GS), indicating that other calcium conductances exist but are not required for the action of Ang II or potassium and currently remain enigmatic.

Besides unraveling the physiology of calcium signaling in the ZG leading to aldosterone productions, our findings also have implications in directing future pharmacological interventions. It has been suggested that the inhibition of T-type calcium channels might represent a promising target for treating hyperaldosteronism (or lowering aldosterone synthesis) in general[16]. Our results, however, imply that a long-term treatment would likely be countered via calcium influx through L-type calcium channels. This explains why mibefradil, a preferential T-type channel inhibitor, did not exert persistent effects on aldosterone levels or blood pressure *in vivo*[39,40]. Nevertheless, a specific blockade of $Ca_V3.2$ or $Ca_V1.3$ in primary aldosteronism due to gain-of-function mutations in either channel may still constitute a therapeutic strategy to alleviate pathological calcium influx into the ZG[11,17,21]. Interestingly, it has been observed in the H295R cell line that a blockade of both, L-

and T-type channels (for example using the unspecific inhibitors benidipine[41] or efonidipine[42]) was efficient in reducing aldosterone production. This may indeed be a strategy to lower aldosterone synthesis, but potential extra-adrenal side effects may limit their usefulness, and this approach therefore requires further investigation.

Material and Methods

Generation and breeding of the *Cacna1h* KO mouse model

Cacna1h KO mice (based on C57BL/6J strain) carrying an 8-bp deletion on exon 25, with subsequent frameshift and termination (p.His1570Glnfs*83, *Cacna1h*$^{+/-}$) were generated previously[11]. *Cacna1h* KO and control mice were bred and housed at the Forschungseinrichtungen für Experimentelle Medizin (FEM; Charité - Universitätsmedizin Berlin) under specific-pathogen free conditions in a 12-h light/dark cycle with *ad libitum* access to food and water.

C57BL/6J mice for single cell RNA-seq experiments were bred and housed at Max Planck Institute for Molecular Genetics (Berlin) and maintained under specific pathogen-free conditions in a 12h light/dark cycle with *ad libitum* access to food and water.

All animal experiments were approved by the local authority (Landesamt für Gesundheit und Soziales Berlin) and performed under consideration of all relevant ethical regulations.

Organ harvest

To harvest adrenal glands for experiments, 10 to 30 week-old mice were anesthetized using isoflurane (400 µL as open drop in a 2-l beaker) and euthanized by cervical dislocation. The abdominal cavity was then opened using scissors, and the adrenal glands identified and rapidly extracted. The procedure of organ harvest following euthanasia was performed according to German law and registered with the local authorities (Landesamt für Gesundheit und Soziales (LaGeSo) Berlin; T 0425/17).

Calcium imaging

For acute slice preparations, similar to previously published procedures[9,11], adrenal glands were transferred into ice cold bicarbonate-buffered saline (BBS: 100 mmol/l NaCl, 2 mmol/l KCl, 26 mmol/l $NaHCO_3$, 0.1 mmol/l $CaCl_2$, 5 mmol/l $MgCl_2$, 10 mmol/l D-glucose, 10 mmol/l HEPES) immediately after extraction. During all following steps, BBS was continuously gassed with carbogen (95 % O_2 + 5 % CO_2). Both glands were embedded into 4 % low-melting agarose, following the removal of the surrounding fat. The organs in the agarose block were

glued to the mounting stage of a vibratome (7000 smz-2, Campden Instruments) and slices were cut at 120 µm thickness. During cutting, adrenal glands in the agarose block and slices were maintained in ice-cold, gassed BBS. Slices were transferred into BBS at 35°C for 15 minutes for regeneration and subsequently stored for up to 6h at RT in BBS supplemented with 2 mmol/l $CaCl_2$.

Slice staining was performed in a cell culture insert within a single well of a 24-well plate at room temperature. The insert was filled with 250 µL containing initially 37 µmol/l Calbryte 520 AM and 0.001 % Pluronic F-127 or 64 µmol/l Fura-2 AM and 0.16 % Pluronic dissolved in BBS (supplemented with 2 mmol/l $CaCl_2$). The well was filled with 750 µL BBS (supplemented with 2 mmol/l $CaCl_2$) and continuously gassed with carbogen. The slices were incubated in the staining solution for 1 h. Following Fura-2 AM staining, slices were transferred to fresh BBS (without Fura-2, supplemented with 2 mmol/l CaCl2) for 15 min de-esterification.

For recording, slices were placed in a recording chamber and were continuously perfused with solution from a reservoir. The solution reservoir was supplied with carbogen gas and was heated via an inline heating coil to a temperature of 30 ± 1°C. Two solutions were prepared and mixed in order to yield the potassium concentration of interest (BBS $2K^+$: 100 mmol/l NaCl, 2 mmol/l KCl, 26 mmol/l $NaHCO_3$, 5 mmol/l NaGluconate, 2 mmol/l $CaCl_2$, 1 mmol/l $MgCl_2$, 10 mmol/l D-glucose, 10 mmol/l HEPES); and BBS $7K^+$: 100 mmol/l NaCl, 2 mmol/l KCl, 26 mmol/l $NaHCO_3$, 5 mmol/l KGluconate, 2 mmol/l $CaCl_2$, 1 mmol/l $MgCl_2$, 10 mmol/l D-glucose, 10 mmol/l HEPES)). Ang II was added from a 1 µmol/l stock to yield final concentrations as indicated.

Calbryte fluorescence was excited at 470 nm while Fura-2 was alternately excited at 340 and 385 nm using a FuraLED light source (Cairn Research). Images were taken every 100 ms with 10-ms exposure using an OptiMOS camera (QImaging).

Electrophysiological recordings of dissociated adrenal cortical cells

For dissociated adrenal cortical cell preparations, extracted adrenal glands were rapidly transferred into bath solution containing 140 mmol/l NaCl, 4 mmol/l KCl, 1 mmol/l $MgCl_2$, 2 mmol/l $CaCl_2$, 10 mmol/l HEPES on ice. After the removal of the surrounding fat, the glands were cut in half and the medulla manually removed. The glands were further cut into fragments (< 0.5 mm) and incubated in bath solution supplemented with collagenase type I

(1mg/ml), collagenase type IV (1mg/ml), penicillin (50 U/ml) and streptomycin (50 mg/ml) for 20 min at 37°C on a shaker set to 300 rpm. Subsequently, shear-based dissociation of the cells was performed in a 1 ml syringe attached to a cannula (18-20 G) and polyethylene tubing (30 cm) of matching diameter. A syringe pump was used to provide a controlled flow rate (700 µL/min) of the cell suspension through the cannula and tubing. The cell suspension was centrifuged for 5 min at 300 g and room temperature. The cell pellet was resuspended in DMEM/F12 (1:1) supplemented with Ultroser G (2 %), penicillin (50 U/ml) and streptomycin (50 mg/ml), α-tocopherol (1 µmol/l), insulin transferrin selenium (1 %), ascorbic acid (100 µmol/l). Cells were seeded on coverslips (9 mm diameter, coated with laminin and poly-L-lysin) in a 24-well plate, incubated in a 5 % CO_2 humidified atmosphere at 37°C and used for whole-cell patch clamp recordings the next day.

Currents were recorded on a HEKA EPC 10 amplifier (HEKA Elektronik) using Patchmaster software. Borosilicate pipettes with resistances of 2–4 MΩ were pulled on a Sutter P-1000 puller (Harvard Apparatus) and subsequently fire polished using a Narishige MF-890 microforge. Extracellular solution contained 100 mmol/l NaCl, TEACl 20 mmol/l, 4 mmol/l KCl, 1 mmol/l $MgCl_2$, 10 mmol/l HEPES, 10 mmol/l $CaCl_2$, pH 7.4. Pipette solution contained 140 mmol/l CsCl, 10 mmol/l NaCl, 5 mmol/l EGTA, 2 mmol/l $MgCl_2$, 10 mmol/l HEPES, pH 7.4. Currents were elicited by voltage steps ranging from either -95 or -55 to 75 mV in 10 mV increments from a holding potential of -80 mV or -40 mV, respectively.

The obtained data was fit with equation 1:

$$[1] \qquad I(V) = G * (V - V_{rev}) * \frac{1}{1+e^{\frac{-(V-V_{0.5})}{k}}}$$

where *I* is the macroscopic current, *G* the maximum conductance, *V* the tested voltage, V_{rev} the reversal potential, $V_{0.5}$ the half-maximal activation and k the slope.

Bulk RNA-seq

For RNA extraction from whole adrenal cortices, extracted adrenal glands from 6 WT and 6 KO (3 male, 3 females each) were rapidly transferred into PBS on ice. After the removal of the surrounding fat, the glands were cut in half, manually separated from the medulla and placed in RNAlater (ThermoFisher). Total RNA was isolated using the RNeasy Mini Kit (Qiagen) with subsequent DNAse digestion according to the manufacturer's instructions.

Purified RNA was then further processed at the Core Unit Genomics of the Berlin Institute of Health at Charité – Universitätsmedizin Berlin. Ribosomal RNA was depleted and cDNA transcribed using the TruSeq Stranded Total RNA kit (Illumina). 150bp paired-end Sequencing was performed on a NovaSeq 6000 device on a single lane of a SP flow cell (all from Illumina).

The complete bioinformatics pipeline used in this study, including all parameters used, can be found on GitHub (https://github.com/dhoangan/Cacna1hKO). In brief, results were analyzed on the background of Ensembl release 106 of the GRCm39 cDNA transcriptome. Indexing of the transcriptome was performed using Salmon[43] (version 1.5.2). Initial quality control of the results was performed using MultiQC[44] (version 1.11). Further quality checks, filtering and trimming was performed using fastp[45] (version 0.12.4). Salmon was also used for mapping of reads. Following inspection, one male KO sample had to be excluded from further analysis as ribosomal RNA made up more than 80 % of all reads, likely because rRNA depletion in the TruSeq Kit failed.

Raw data from our bulk RNA-seq experiment can be accessed at ArrayExpress with the accession number E-MTAB-12999 (https://www.ebi.ac.uk/biostudies/arrayexpress/studies/E-MTAB-12999).

Filtered gene counts were further processed and analyzed using DESeq2[46] (version 1.38.3) in R (version 4.2.1). Differentially expressed genes (DEGs) were identified using the DESeq function with the chosen threshold criteria of p-values < 0.05 (adjusted using the Benjamini–Hochberg correction) and a 2-fold change (log2 transformed fold change ± 1, after shrinkage using the apeglm method[47]). Filtered gene counts were further processed and analyzed using DESeq2[46] (version 1.38.3) in R (version 4.2.1). Differentially expressed genes (DEGs) were identified using the DESeq function with the chosen threshold criteria of p-values < 0.05 (adjusted using the Benjamini–Hochberg correction) and a 2-fold change (log2 transformed fold change ± 1).

For heatmap generation, raw read counts were normalized using the DESeq2. If indicated, a Z-score normalization was performed on the normalized read counts across samples for each gene.

Functional enrichment analysis of the identified DEGs was assessed based on Gene Ontology[48] (GO) and KEGG pathway[49] over-representation using the ClusterProfiler[50]

package (version 4.6.2) in R. A gene set enrichment analysis over the full data set was also performed using the ClusterProfiler package. A p-value less than 0.05 was considered as statistically significant.

Single cell RNA-seq

After adult mice (two males and two females; each seven weeks old) were killed by cervical dislocation, both adrenal glands were collected, snap frozen in liquid nitrogen and stored at -80°C until further procedures.

Adrenal glands were processed using a dounce homogenizer in a Triton X-100 lysis buffer (10% Triton X-100, Superasin 20 U/µL, RNAseIn U/µl, Nuclei Isolation Medium: 1mM DTT, 50X Protease Inhibitor, 1.5M Sucrose, 1M KCL, 1M $MgCl_2$, 1M Tris buffer pH 8.0) to get a nuclei suspension. Subsequently, the suspension was stained with DAPI (4',6-diamidino-2-phenylindole) and sorted by flow cytometry (BD FACSAria III High Sensitivity Flow Cytometer (mouse), BD Genomics, USA) into RNAse inhibitor containing tubes. The nuclei quality was assessed under Leica DMi8 microscope and quantified using a Neubauer chamber.

Each single-nuclei suspension was loaded onto a Chromium Single Cell 3'Chip A (10X Genomics) to yield GEMs (Gel Beads in Emulsion). Subsequently, GEMs were processed according to Chromium Single Cell 3' Reagent Kits v3 (CG000183 Rev C), to generate sequencing-ready libraries. Libraries were sequenced on an Illumina HiSeq 4000 following 10X Genomics sequencing guidelines.

All count matrices were processed with Seurat using *CreateSeuratObject* function (*min.cells = 3, min.features = 200*): further filtering was performed during QC step, by filtering cells less than 700 genes (*nFeature_RNA > 700*) and outliers with over 10,000 UMIs were removed (*nCount_RNA < 10,000*). Next, filtered matrices were merged (ncells = 27,448) and normalization was performed using *SCTransform*(2), regressing out cell cycle and the overexpressed *Malat1* gene (*vars.to.regress = c("malat","S.Score","G2M.Score"*) in the process. After PCs were computed (*RunPCA*), UMAP was generated with the first 30 PCs (*RunUMAP*). Clustering and cell type identification was conducted using cNMF(3): briefly, a total of 10 gene expression programs (GEPs) were produced, and a "usage" matrix was created to indicate the extent to which each GEP contributes to a cell's identity. Each cell was assigned a discrete cluster identity based on the highest usage score obtained. Differentially expressed genes were then computed using *FindAllMarkers* (*test.use = "LM"*,

latent.vars = "nCount_RNA"), and the annotations of each cluster was done by cross-referencing their top expressed genes with established markers from literature.

Gene expression program 8 had canonic ZG markers such as *Dab2* (Disabled homolog 2), *Cacnb2* (Calcium voltage-gated channel auxiliary subunit beta 2), *Agtr1b* (Angiotensin II receptor, type 1b) and *Agtr1a* (Angiotensin II receptor, type 1b), therefore we identified cells with a high GEP 8 score as ZG. Using the subset() function, we extracted 6589 ZG cells.

Statistics

All P-values (except for the differential expression analysis) are results from a likelihood ratio test of the linear mixed models and are indicated as follows: ns, $P \geq 0.05$; *, <0.05; **, P<0.01; ***, P<0.001. Statistical mixed model analysis was performed in R (4.2.1) using the glmmTMB package (version 1.1.5). Normality of the data was assured visually using quartile-quartile plots and inspection of residuals after fitting. If data was not normally distributed, a diverse set of distributions was tested using DHARMa (version 0.4.6), and either the log-Tweedie or log-Gamma distribution was chosen for further analysis using glmmTMB. Individual recordings were treated as random effect. All error bars and bands show 95% confidence interval of the mean value.

For differential expression analysis, reads obtained by RNA sequencing were normalized and differentially analyzed using the DESeq2 package (version 1.38.3). Genes were considered as significantly regulated with the chosen threshold criteria of a 2-fold change (log2-transformed fold change ± 1) and a P-value lower than 0.05 (adjusted by Benjamini–Hochberg procedure for multiple comparisons).

Acknowledgements

We would like to thank the team of the Core Unit Genomics of the Berlin Institute of Health at Charité – Universitätsmedizin Berlin, in particular Dr. Tatiana Borodina, for performing library preparation and sequencing of our RNA samples. We are very grateful to Sarah Döring, Nico Brüssow, Marie Cotta and Ana Lucia Huitron Carrizales for performing mouse genotyping. The authors also would like to thank Drs. Julia Schewe and Eric Seidel for their help with establishing the Cacna1h$^{-/-}$ colony. This work was supported by the Deutsche Forschungsgemeinschaft (STO 1260/1-1 to GS) and the Stiftung Charité (BIH Johanna Quandt Professorship to UIS).

Author Contributions

G.S. conceived the study; H.A.D. and M.V. performed calcium imaging; H.A.D. and G.S. analyzed calcium imaging data; H.A.D. and G.S. analyzed bulk RNA-seq data; H.A.D. performed and analyzed patch clamp experiments of adrenocortical cells; A.K.S. and U.I.S. designed single nucleus RNA-seq experiments; A.K.S. performed and analyzed single nucleus RNA-seq experiments; H.A.D, U.I.S. and G.S. wrote the manuscript with contributions from all authors.

Competing Interests

None of the authors declare any competing interests.

References

1. Hattangady, N., Olala, L., Bollag, W. B. & Rainey, W. E. Acute and Chronic Regulation of Aldosterone Production. *Mol Cell Endocrinol* **350**, 151–162 (2012).
2. Monticone, S. *et al.* Prevalence and Clinical Manifestations of Primary Aldosteronism Encountered in Primary Care Practice. *Journal of the American College of Cardiology* **69**, 1811–1820 (2017).
3. Capponi, A. M., Lew, P. D., Jornot, L. & Vallotton, M. B. Correlation between cytosolic free Ca2+ and aldosterone production in bovine adrenal glomerulosa cells. Evidence for a difference in the mode of action of angiotensin II and potassium. *J Biol Chem* **259**, 8863–8869 (1984).
4. Spät, A. & Hunyady, L. Control of Aldosterone Secretion: A Model for Convergence in Cellular Signaling Pathways. *Physiological Reviews* **84**, 489–539 (2004).
5. Penton, D. *et al.* Task3 Potassium Channel Gene Invalidation Causes Low Renin and Salt-Sensitive Arterial Hypertension. *Endocrinology* **153**, 4740–4748 (2012).
6. Heitzmann, D. *et al.* Invalidation of TASK1 potassium channels disrupts adrenal gland zonation and mineralocorticoid homeostasis. *The EMBO Journal* **27**, 179–187 (2008).
7. Ely, J. A. *et al.* Relationship between agonist- and thapsigargin-sensitive calcium pools in adrenal glomerulosa cells. Thapsigargin-induced Ca2+ mobilization and entry. *J. Biol. Chem.* **266**, 18635–18641 (1991).
8. Hajnóczky, G. *et al.* Thapsigargin-Induced Increase in Cytoplasmic Ca2+ Concentration and Aldosterone Production in Rat Adrenal Glomerulosa Cells: Interaction with Potassium and Angiotensin-II. *Endocrinology* **128**, 2639–2644 (1991).
9. Schewe, J. *et al.* Elevated aldosterone and blood pressure in a mouse model of familial hyperaldosteronism with ClC-2 mutation. *Nature Communications* **10**, 5155 (2019).
10. Guagliardo, N. A. *et al.* Angiotensin II induces coordinated calcium bursts in aldosterone-producing adrenal rosettes. *Nat Commun* **11**, 1–15 (2020).
11. Seidel, E. *et al.* Enhanced Ca2+ signaling, mild primary aldosteronism, and hypertension in a familial hyperaldosteronism mouse model (Cacna1hM1560V/+). *PNAS* **118**, (2021).
12. Clyne, C. D., White, P. C. & Rainey, W. E. Calcium regulates human CYP11B2 transcription. *Endocr Res* **22**, 485–492 (1996).

13. Yagci, A. & Müller, J. Induction of steroidogenic enzymes by potassium in cultured rat zona glomerulosa cells depends on calcium influx and intact protein synthesis. *Endocrinology* **137**, 4331–4338 (1996).
14. Kowluru, R., Yamazaki, T., McNamara, B. C. & Jefcoate, C. R. Metabolism of exogenous cholesterol by rat adrenal mitochondria is stimulated equally by physiological levels of free Ca2+ and by GTP. *Molecular and Cellular Endocrinology* **107**, 181–188 (1995).
15. Hu, C., Rusin, C. G., Tan, Z., Guagliardo, N. A. & Barrett, P. Q. Zona glomerulosa cells of the mouse adrenal cortex are intrinsic electrical oscillators. *Journal of Clinical Investigation* **122**, 2046–2053 (2012).
16. Rossier, M. F., Ertel, E. A., Vallotton, M. B. & Capponi, A. M. Inhibitory action of mibefradil on calcium signaling and aldosterone synthesis in bovine adrenal glomerulosa cells. *J Pharmacol Exp Ther* **287**, 824–831 (1998).
17. Scholl, U. I. *et al.* Somatic and germline CACNA1D calcium channel mutations in aldosterone-producing adenomas and primary aldosteronism. *Nat Genet* **45**, 1050–1054 (2013).
18. Scholl, U. I. *et al.* Recurrent gain of function mutation in calcium channel CACNA1H causes early-onset hypertension with primary aldosteronism. *eLife Sciences* **4**, e06315 (2015).
19. Yang, T., He, M., Zhang, H., Barrett, P. Q. & Hu, C. L- and T-type calcium channels control aldosterone production from human adrenals. *Journal of Endocrinology* **244**, 237–247 (2020).
20. Barrett, P. Q., Guagliardo, N. A. & Bayliss, D. A. Ion Channel Function and Electrical Excitability in the Zona Glomerulosa: A Network Perspective on Aldosterone Regulation. *Annu. Rev. Physiol.* (2020) doi:10/ghj4zw.
21. Azizan, E. A. B. *et al.* Somatic mutations in ATP1A1 and CACNA1D underlie a common subtype of adrenal hypertension. *Nature Genetics* **45**, 1055–1060 (2013).
22. Thuesen, A. D. *et al.* Deficiency of T-type Ca^{2+} channels $Ca_v3.1$ and $Ca_v3.2$ has no effect on angiotensin II-induced hypertension but differential effect on plasma aldosterone in mice. *American Journal of Physiology-Renal Physiology* **317**, F254–F263 (2019).
23. Nogueira, E. F. & Rainey, W. E. Regulation of Aldosterone Synthase by Activator Transcription Factor/cAMP Response Element-Binding Protein Family Members. *Endocrinology* **151**, 1060–1070 (2010).
24. Stölting, G. *et al.* Direct Interaction of CaVβ with Actin Up-regulates L-type Calcium Currents in HL-1 Cardiomyocytes. *J. Biol. Chem.* **290**, 4561–4572 (2015).
25. Shipe, W. D. *et al.* Design, Synthesis, and Evaluation of a Novel 4-Aminomethyl-4-fluoropiperidine as a T-Type Ca2+ Channel Antagonist. *J. Med. Chem.* **51**, 3692–3695 (2008).
26. Choe, W. *et al.* TTA-P2 Is a Potent and Selective Blocker of T-Type Calcium Channels in Rat Sensory Neurons and a Novel Antinociceptive Agent. *Mol Pharmacol* **80**, 900–910 (2011).
27. Ortner, N. J. *et al.* Lower Affinity of Isradipine for L-Type Ca2+ Channels during Substantia Nigra Dopamine Neuron-Like Activity: Implications for Neuroprotection in Parkinson's Disease. *J. Neurosci.* **37**, 6761–6777 (2017).
28. Hockerman, G. H. *et al.* Construction of a high-affinity receptor site for dihydropyridine agonists and antagonists by single amino acid substitutions in a non-l-type Ca2+ channel. *Proceedings of the National Academy of Sciences* **94**, 14906–14911 (1997).
29. Lin, M., Aladejebi, O. & Hockerman, G. H. Distinct properties of amlodipine and nicardipine block of the voltage-dependent Ca2+ channels Cav1.2 and Cav2.1 and the mutant channels Cav1.2/Dihydropyridine insensitive and Cav2.1/Dihydropyridine sensitive.

European Journal of Pharmacology **670**, 105–113 (2011).
30. Zamponi, G. W. Antagonist binding sites of voltage-dependent calcium channels. *Drug Development Research* **42**, 131–143 (1997).
31. Fernandes-Rosa, F. L. *et al.* Genetic Spectrum and Clinical Correlates of Somatic Mutations in Aldosterone-Producing Adenoma. *Hypertension* **64**, 354–361 (2014).
32. De Sousa, K. *et al.* Genetic, Cellular, and Molecular Heterogeneity in Adrenals With Aldosterone-Producing Adenoma. *Hypertension* **75**, 1034–1044 (2020).
33. Nishimoto, K. *et al.* Transcriptome Analysis Reveals Differentially Expressed Transcripts in Rat Adrenal Zona Glomerulosa and Zona Fasciculata. *Endocrinology* **153**, 1755–1763 (2012).
34. Xie, C. B. *et al.* Regulation of aldosterone secretion by $Ca_v1.3$. *Scientific Reports* **6**, 24697 (2016).
35. Enyeart, J. J. & Enyeart, J. A. Human adrenal glomerulosa cells express K2P and GIRK potassium channels that are inhibited by ANG II and ACTH. *American Journal of Physiology-Cell Physiology* **321**, C158–C175 (2021).
36. Payet, M. D., Durroux, T., Bilodeau, L., Guillon, G. & Gallo-Payet, N. Characterization of K+ and Ca2+ ionic currents in glomerulosa cells from human adrenal glands. *Endocrinology* **134**, 2589–2598 (1994).
37. Gancayco, C. A. *et al.* Intrinsic Adrenal TWIK-Related Acid-Sensitive Potassium Channel Dysfunction Produces Spontaneous Calcium Oscillations Sufficient to Drive AngII (Angiotensin II)-Unresponsive Hyperaldosteronism. *Hypertension* **0**, 10.1161/HYPERTENSIONAHA.122.19557.
38. Yang, T. *et al.* Small-Conductance Ca2+-Activated Potassium Channels Negatively Regulate Aldosterone Secretion in Human Adrenocortical Cells. *Hypertension* (2016) doi:10/f83499.
39. Schmitt, R. *et al.* Hemodynamic and humoral effects of the novel calcium antagonist Ro 40-5967 in patients with hypertension. *Clinical Pharmacology & Therapeutics* **52**, 314–323 (1992).
40. Ragueneau, I. *et al.* Comparison of sympathetic modulation induced by single oral doses of mibefradil, amlodipine, and nifedipine in healthy volunteers. *Clinical Pharmacology & Therapeutics* **69**, 122–129 (2001).
41. Akizuki, O. *et al.* Blockade of T-type voltage-dependent Ca2+ channels by benidipine, a dihydropyridine calcium channel blocker, inhibits aldosterone production in human adrenocortical cell line NCI-H295R. *European Journal of Pharmacology* **584**, 424–434 (2008).
42. Imagawa, K. *et al.* Inhibitory Effect of Efonidipine on Aldosterone Synthesis and Secretion in Human Adrenocarcinoma (H295R) Cells. *Journal of Cardiovascular Pharmacology* **47**, 133 (2006).
43. Patro, R., Duggal, G., Love, M. I., Irizarry, R. A. & Kingsford, C. Salmon provides fast and bias-aware quantification of transcript expression. *Nat Methods* **14**, 417–419 (2017).
44. Ewels, P., Magnusson, M., Lundin, S. & Käller, M. MultiQC: summarize analysis results for multiple tools and samples in a single report. *Bioinformatics* **32**, 3047–3048 (2016).
45. Chen, S., Zhou, Y., Chen, Y. & Gu, J. fastp: an ultra-fast all-in-one FASTQ preprocessor. *Bioinformatics* **34**, i884–i890 (2018).
46. Love, M. I., Huber, W. & Anders, S. Moderated estimation of fold change and dispersion for RNA-seq data with DESeq2. *Genome Biology* **15**, 550 (2014).
47. Zhu, A., Ibrahim, J. G. & Love, M. I. Heavy-tailed prior distributions for sequence count data: removing the noise and preserving large differences. *Bioinformatics* **35**, 2084–2092 (2019).

48. Ashburner, M. *et al.* Gene Ontology: tool for the unification of biology. *Nat Genet* **25**, 25–29 (2000).
49. Kanehisa, M. & Goto, S. KEGG: Kyoto Encyclopedia of Genes and Genomes. *Nucleic Acids Research* **28**, 27–30 (2000).
50. Wu, T. *et al.* clusterProfiler 4.0: A universal enrichment tool for interpreting omics data. *The Innovation* **2**, 100141 (2021).